Nickel electrowinning using a Pt catalysed hydrogen-diffusion anode. Part I: Effect of chloride and sulfate ions and a magnetic field

E. BRILLAS[1], J. RAMBLA[1] and J. CASADO[2]

[1]*Laboratori de Ciència i Tecnologia Electroquímica de Materials, Departament de Química Física, Facultat de Química, Universitat de Barcelona, Martí i Franquès 1-11, 08028 Barcelona, Spain*
[2]*Departamento de Investigación, Carburos Metálicos S.A., P° Zona Franca 14-20, 08038 Barcelona, Spain*

Abstract

The use of a Pt catalysed H_2-diffusion anode for Ni electrowinning has been studied from typical chloride, Watts and sulfate baths at 25 °C. Higher anodic current densities are found in a three-electrode cell when sulfate ions are gradually replaced by chloride ions. Adherent Ni deposits are obtained from the Watts and sulfate media, whereas in the chloride bath, Cl_2 is released at the anode and less adherent deposits are formed. Current efficiencies between 94% and 98% for anodic current densities ranging from 15 to 65 mA cm^{-2} have been found. The energy costs for Ni electrowinning decrease with increasing chloride content in the bath, and their values are always much lower than those reported using conventional DSA, graphite or lead anodes. All deposits are composed of high-purity Ni, free of heavy metals and other impurities. The crystals have a face-centred cubic structure with a preferential orientation which mainly depends on the medium and current density. A superimposed magnetic field of 0.9 T orientated either parallel or perpendicular to electrodes in a two-electrode cell exerts only a small effect on the crystallographic orientation of Ni, although it has a certain influence on its morphology.

1. Introduction

Electrowinning is one of the most important procedures for the production of high-purity nickel for technical and industrial applications involving sectors such as spacecraft engineering, aviation and electronics. Operating cells contain a Ni stationary or rotating cathode, a DSA, graphite or lead anode and a bath prepared with $NiCl_2$ and/or $NiSO_4$, usually in the presence of a high concentration of boric acid [1–3]. The buffering action of boric acid at the cathode surface favours the deposition process, since it causes a decrease in the H_2-evolution rate [4] and a lower precipitation of insoluble $Ni(OH)_2$ [5]. The main disadvantages of these cells are the high voltages applied and the contamination of deposits with small amounts of inorganic impurities, such as lead, iron, cobalt, copper and sulfur [6]. Recently, Nikolova et al. [7] have reported that the use of an alternative H_2-diffusion anode catalysed by tungsten carbide causes a considerable decrease in the electrical energy cost, along with the production of Ni free of heavy metal impurities due to the high corrosion resistance of the catalyst. The properties of other H_2-diffusion anodes with different stable catalysts should then be tested to establish whether they can replace the conventional anodes for Ni electrowinning. The purity, structure and morphology of the deposits obtained are

also important factors in deciding the possible technological applicability of these diffusion anodes.

Several workers have studied the crystallographic orientation and deposit morphology of Ni produced from chloride, Watts (containing $NiCl_2$, $NiSO_4$ and H_3BO_3) and sulfate baths [6, 8–12] with conventional anodes. The authors describe the formation of simple cubic or face-centred cubic structures, showing that the grain size, surface morphology and preferred orientation of deposits depend on both the electrolysis conditions and the electrolyte composition. These effects on the growth mode of the crystals are associated with the selective adsorption of different inhibitors, such as H_2, $H^.$ or $Ni(OH)_2$, in the Ni-electrolyte interface during the deposition process [10, 11].

On the other hand, contradictory results have been reported [9, 13–15] when an external magnetic field is applied during Ni electrowinning at constant current density j. Although Yang [13] did not find any effect on the crystal orientation in the presence of a magnetic field of 0.54 T at $j = 12.5$ mA cm^{-2}, Chiba et al. [9] observed large effects on the Ni texture operating up to 0.15 T at $j = 15$ mA cm^{-2}. Danilyuk et al. [14] have explained these contradictory observations considering that certain values of the magnetic field accelerate the electrodeposition reaction, whereas others cause its inhibition, thus changing the Ni morphology. Recently, Devos et al. [16]

have reported that a uniform magnetic field close to 1 T parallel to the cathode surface changes the morphology and the preferential growth direction of Ni obtained at constant cathodic potentials from a Watts solution.

The aim of this work is to study the feasibility of using a Pt catalysed H_2-diffusion anode for the production of high-purity Ni with low energy cost from typical chloride, Watts and sulfate baths employed in electrowinning. The crystallographic orientation and surface morphology of deposits formed at different current densities, in the absence and presence of a uniform magnetic field of 0.9 T, have been examined to establish the most favourable electrodeposition conditions. The current–potential plots for the anode, as well as the current efficiency and energy cost for the process, have been determined using a three-electrode cell. A smaller two-electrode cell has been employed to investigate the influence of the magnetic field orientated either parallel or perpendicular to electrodes.

2. Experimental details

2.1. Solutions and reagents

Nickel was electrodeposited from the following electrolytes: chloride bath with 300 g L^{-1} $NiCl_2.6 H_2O$ + 35 g L^{-1} H_3BO_3 (pH 3.0); Watts bath containing 300 g L^{-1} $NiSO_4.7 H_2O$ + 45 g L^{-1} $NiCl_2.6 H_2O$ + 35 g L^{-1} H_3BO_3 (pH 3.6); sulfate bath with 300 g L^{-1} $NiSO_4.7 H_2O$ + 35 g L^{-1} H_3BO_3 (pH 3.8). These solutions were prepared with analytical grade chemicals supplied by Merck and Probus, using water obtained from a Millipore Milli-Q system, with a conductivity lower than 6×10^{-8} Ω^{-1} cm^{-1}.

2.2. Preparation of the Pt catalysed H_2-diffusion anode

The H_2-diffusion anode was composed of two carbon-PTFE layers stacked onto a Ni screen of 125 mesh and 0.11 mm thickness as current collector. The inner layer in contact with the Ni screen served as H_2-supply to the reactive outer layer with Pt as catalyst. Carbon blacks Printex L (surface area 136 m^2 g^{-1}) and Printex XE-2 (surface area 912 m^2 g^{-1}) from Degussa were used for the inner and reactive layers, respectively. A 7% w/w Pt was deposited on the Printex XE-2 from reduction of H_2PtCl_6 with formaldehyde [17]. The uncatalysed and catalysed layers were prepared from the following procedure [18]. About 1 g of Printex L or 1 g of Printex XE-2 + 7% Pt was suspended in 100 mL of water with 3% w/w n-butanol as dispersant. Further, 0.25 g of PTFE 30-N dispersion from Du Pont de Nemours was added and mixed. This suspension was heated at 80 °C for 12 h to evaporate the water and the residuum was dried at 240 °C for 3 h. The resulting cake was pulverized into fine powders with a mill. Adjacent layers of the inner (120 mg) and reactive (90 mg) carbon-PTFE powders were cold-pressed at 130 kg cm^{-2} onto a Ni

screen of 2.5 cm diameter between two laminated steel cylinders, and further hot-pressed under the same pressure at 400 °C for 10 min. The thickness of the anode thus prepared was 0.53 mm. A nichrome wire was welded to the Ni screen for electrical connection.

2.3. Three-electrode cell

Electrochemical experiments without magnetic field were carried out with a three-electrode thermostated cell of 100 mL capacity, using an Amel 555A potentiostat–galvanostat connected to an Amel 721 current integrator. The H_2-diffusion anode was placed at the bottom of a cylindric holder of polypropylene, where its area was limited to 3.1 cm^2. It became operative when pure H_2 gas at 40 ml min^{-1} was passed over its inner face through a glass tube inside the holder, the top of which was open to atmosphere. The cathode was a Ti/Ni electrode consisting of a polished titanium foil (2.0 cm × 2.5 cm × 0.1 cm in dimension from Inagasa) coated with a thin and adherent layer of Ni obtained by pre-electrolysing the solution tested at 30 mA for 5 min. The interelectrode gap was close to 2 cm. The reference electrode was a Ag/AgCl electrode with a NaCl-saturated aqueous solution ($E° = 0.203$ V at 25 °C).

All experiments were carried out by applying a constant anodic potential, E_{anod}, and determining the anodic current density j_{anod}. The cell voltage, V, was measured with a Demestres 605 digital multimeter. In some cases, the electrolyte was stirred with a magnetic bar at constant rotation speed regulated with a Schott MR 1160 stirrer. The behaviour of the anode was monitored from the $j_{anod} - E_{anod} - V$ plots at different temperatures, with or without solution stirring. Electrolyses were performed at different E_{anod} values for 1 h. The evolution of j_{anod} and V with time was followed to calculate the current efficiency and energy consumption from the weight of recovered Ni. The overall electrical charge consumed was obtained from the current integrator.

2.4. Electrolytic system with external magnetic field

The possible effect of a magnetic field on Ni electrowinning was studied with a PM-900-45 permanent magnet system from the Group of Magnetic Solutions of Trinity College of Dublin. It consists of a metallic cylinder of 17.5 cm diameter and 14 cm height with a central hole of 4.5 cm diameter, where a uniform magnetic field of 0.9 T can be applied to a cell placed in it with an orientation parallel or perpendicular to its electrodes. The cell was a cylindric tube of 4.3 cm diameter and 12 cm height containing two parallel vertical electrodes separated 1.5 cm. The anode was a Pt catalysed H_2-diffusion electrode. The cathode was a stainless steel disc (a soft magnetic material) of 2.5 cm diameter and 0.1 cm thickness coated with Ni electrodeposited from each electrolyte at 30 mA for 5 min. Each electrode was welded to a nichrome wire and put into a PVC holder, where its area was limited to 3.1 cm^2. The holder of the

anode had a small gas chamber in contact with its inner face and open to atmosphere. The anode became operative when pure H_2 gas at 40 ml min^{-1} was circulated through this chamber.

A volume of 50 ml of each bath was electrolysed in the two-electrode cell for 1 h at room temperature (23 ± 2 °C) by applying a constant current density j with a Hewlett-Packard HP6545A power supply. The cell voltage was measured with a Schlumberger Solartron 7055 microprocessor voltmeter. The surface morphology of Ni deposits was examined by SEM with a Cambridge Stereoscan S-120 scanning electron microscopy. This instrument was also used to determine the deposit purity by energy dispersive X-ray spectrometry (EDS). The crystallographic orientations were obtained by X-ray diffraction (XRD) with a Siemens D-500 Bragg-Brentano $\theta/2\theta$ geometry powder diffractometer.

3. Results and discussion

3.1. Electrochemical behaviour of the Pt catalysed H_2-diffusion anode

The effect of electrolyte composition on the steady current density at the H_2-diffusion anode in the three-electrode cell at different anodic potentials and cell voltages is shown in Figures 1 and 2, respectively. Hydrogen gas is always oxidized to protons from an anodic potential of about -300 mV, when the cell voltage is near 0.3 V. At given E_{anod} or V values, the higher anodic current density is found for the chloride bath (curves (a)), whereas the j_{anod} value for the Watts bath (curves (b)) is slightly higher than that of the sulfate one (curves (c)). For example, at 2.1 V (Figure 2), anodic current densities of 110, 57 and 44 mA cm^{-2} are obtained for the chloride, Watts and sulfate media,
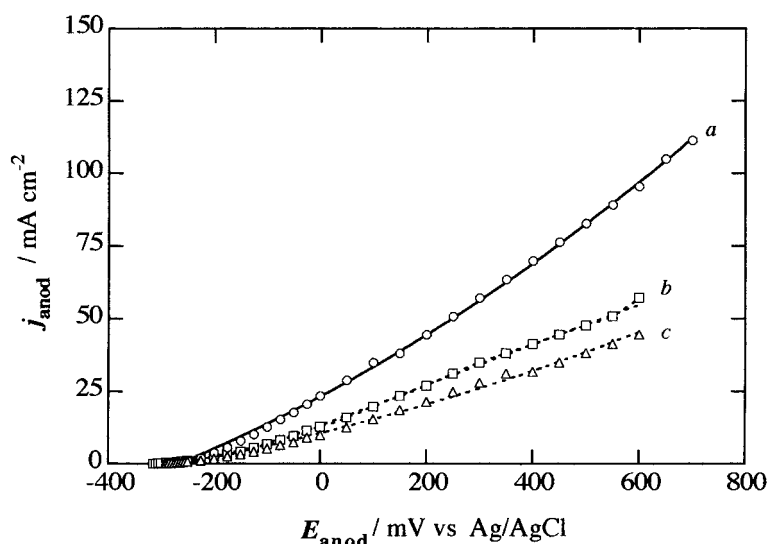

Fig. 1. Current density vs. potential plots for a Pt catalysed H_2-diffusion anode (3.1 cm^2) in a three-electrode cell for Ni electrowinning with a Ti/Ni cathode (10 cm^2) and an electrolyte volume of 100 ml. (a) Chloride bath; (b) Watts bath; (c) sulfate bath. Temperature 25 °C.
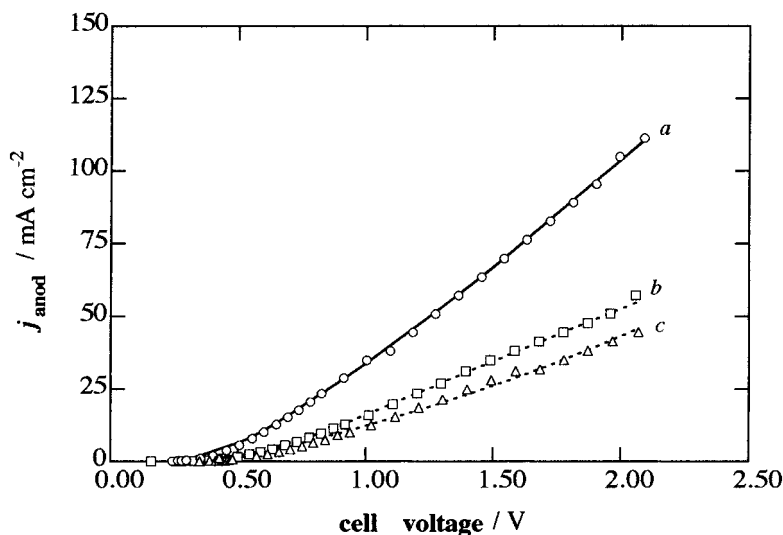

Fig. 2. Dependence of anodic current density on cell voltage under the same conditions as given in Figure 1.

respectively. This trend may be due to the lower ohmic drop of the electrolyte as sulfate ions are being replaced by chloride ions. The increase in chloride content then favours the overall process. In addition, the linear portions of the curves in Figures 1 and 2 indicate ohmic control at sufficiently high currents. Note that a Pt catalysed H_2-diffusion anode gives much higher current densities than those reported for DSA, graphite or lead anodes [1–3]. Cells with these conventional anodes and chloride baths at 50–60 °C usually work between 20 and 30 mA cm^{-2} with voltages between 3.0 and 3.6 V.

The influence of temperature and solution stirring on the j_{anod}/E_{anod} plots for the Watts bath is shown in Figure 3. At a given E_{anod}, a higher j_{anod} value is found at 35 °C (Figure 3(a)) than at 25 °C (Figure 3(b)) without stirring. This can be explained by the expected decrease in ohmic drop of the electrolyte. The same behaviour is observed for the other baths. However, when electrolytes were stirred, no significant change in j_{anod} was found. For $E_{anod} > 200$ mV, a slightly lower anodic current density is detected at 600 rpm (Figure 3(c)) than under quiescent conditions (Figure 3(b)). This rules out a control of the overall process by the transport of reactants towards the electrodes (H_2 gas to the anode and Ni^{2+} to the cathode), in agreement with the suggested ohmic control. From these results, the further experiments were carried out with quiescent baths.

3.2. Nickel electrowinning

All baths were electrolysed in the three-electrode cell at different constant anodic potentials from 0 mV to 600 mV for 1 h at 25 °C. Adherent Ni deposits were always obtained from the Watts and sulfate media. For the chloride bath, however, an increasing evolution of Cl_2 at the anode proceeding from the oxidation of Cl^- was detected as E_{anod} increased, giving rise to deposits of low adherence. In all cases, the solution pH progres-sively decreases due to the continuous production of protons at the anode. At 600 mV, a maximum variation close to 1 pH unit is found for the Watts and sulfate media. The gradual increase in acidity of baths causes a decrease in their ohmic drop and a progressive increase in current density. This phenomenon becomes more significant from $j_{anod} > 40$ mA cm^{-2}, as can be seen in Figure 4 for quiescent Watts baths. In contrast, the cell voltage, which also increases with increasing E_{anod}, remains practically constant.

The current efficiency for each bath after 1 h of electrolysis at average j_{anod} values between 15 and 65 mA cm^{-2} is shown in Figure 5. Good efficiencies between 94% and 98% are always found. From these data and the weights of Ni deposits, the average energy cost for each experiment was calculated. Figure 6 shows a linear increase of the cost with the anodic current density, although its value depends on the electrolyte, decreasing in the order sulfate bath $\geqslant$ Watts bath > chloride bath, in agreement with the $j_{anod} - E_{anod} - V$ behaviour of the system established from Figures 1 and 2.

Electrolyses at longer times were also attempted for the Watts and sulfate media at $j_{anod} > 30$ mA cm^{-2} without pH regulation, but when the pH was lower than 2, lower efficiencies and less adherent deposits were obtained. Under these conditions, the H_2 evolution increases and the buffering action of boric acid on the cathode surface is inefficient [4]. These results agree with those of Nikolova et al. [7], who reported an optimum pH range between 2 and 4 for Ni electrowinning from a sulfate medium using a flow cell with a H_2-diffusion anode catalysed by tungsten carbide.

Results of Figure 6 show that at $j_{anod} \approx 35$ mA cm^{-2} and at 25 °C, costs of about 0.8 kWh kg^{-1} for the chloride bath and close to 1.4 kWh kg^{-1} for both Watts and sulfate media are obtained with the Pt catalysed H_2-diffusion anode. In contrast, consumptions as high as 3 kWh kg^{-1} and efficiencies between 92% and 99%
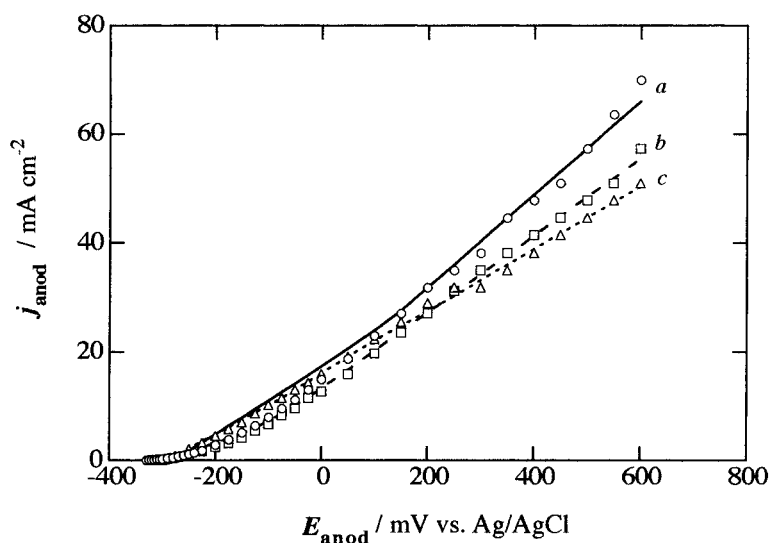

Fig. 3. Variation of current density with potential for a Pt catalysed H_2-diffusion anode (3.1 cm^2) in a three-electrode cell with 100 ml of a Watts bath. Temperature: (a) 35 °C; (b, c) 25 °C. In (c) the electrolyte was stirred at 600 rpm with a magnetic bar.
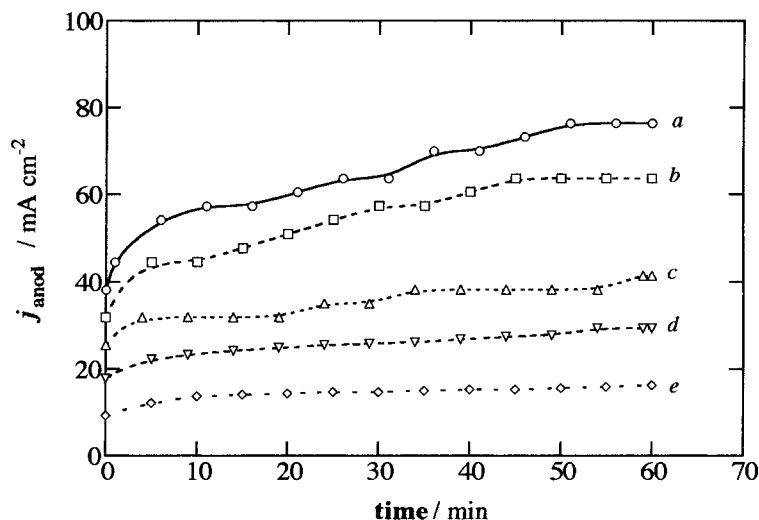
Fig. 4. Evolution of anodic current density during 1 h of Ni electrodeposition on a Ti/Ni cathode (10 cm^2) in a three-electrode cell with a Pt catalysed H$_2$-diffusion anode (3.1 cm^2) and 100 ml of a Watts bath. Anodic potential: (a) 600; (b) 450; (c) 300; (d) 150, (e) 0 mV vs Ag/AgCl. Temperature 25 °C.
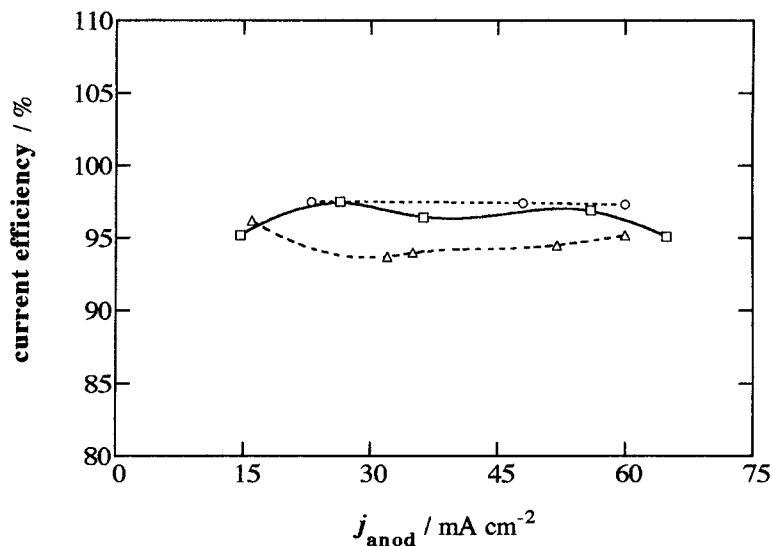

Fig. 5. Variation of current efficiency with average anodic current density after 1 h of Ni electrowinning on a Ti/Ni cathode (10 cm^2) using a Pt catalysed H$_2$-diffusion anode (3.1 cm^2) in a three-electrode cell. Electrolyte volume 100 ml. (O) Chloride bath; (□) Watts bath; (△) sulfate bath. Temperature 25 °C.

have been reported for DSA or graphite anodes using a chloride bath at 30 mA cm^{-2} and at 50–60 °C [1–3]. A higher energy cost of 4.3 kWh kg^{-1} with an efficiency of 96% have been described for a sulfate bath electrolysed with a lead anode at 40 mA cm^{-2} and at 60 °C [6]. The Pt catalysed H$_2$-diffusion anode then gives much lower energy consumptions for Ni electrowinning than conventional anodes.

It is noteworthy that Pt behaves in a similar way to tungsten carbide as catalyst for the oxidation of H$_2$ to protons. For a H$_2$-diffusion anode with tungsten carbide [7], an optimum energy cost of 1.5 kWh kg^{-1} with an efficiency of 99% were obtained for a sulfate medium at 40 mA cm^{-2} and at 70 °C, values very close to those determined with the Pt catalyst at 25 °C (Figures 5 and 6).

3.3. *Effect of a magnetic field on nickel electrowinning*

Comparative electrolyses were carried out using a two-electrode cell with a Pt catalysed H$_2$-diffusion anode and a stainless steel/Ni cathode, both of 3.1 cm^2 area, placed inside the permanent magnet system. For each bath, constant current densities of 10, 30 and 50 mA cm^{-2} were applied for 1 h at room temperature, and at a given *j*, several experiments were performed without magnetic field and with the field of 0.9 T orientated in a direction either parallel or perpendicular to electrodes. The deposits were carefully rinsed with water and dried by hot air to constant weight before analysis by EDS, XRD and SEM.

When baths are electrolysed, they become gradually more acidic, achieving the same final pH in the presence and absence of the magnetic field. For example, final pH
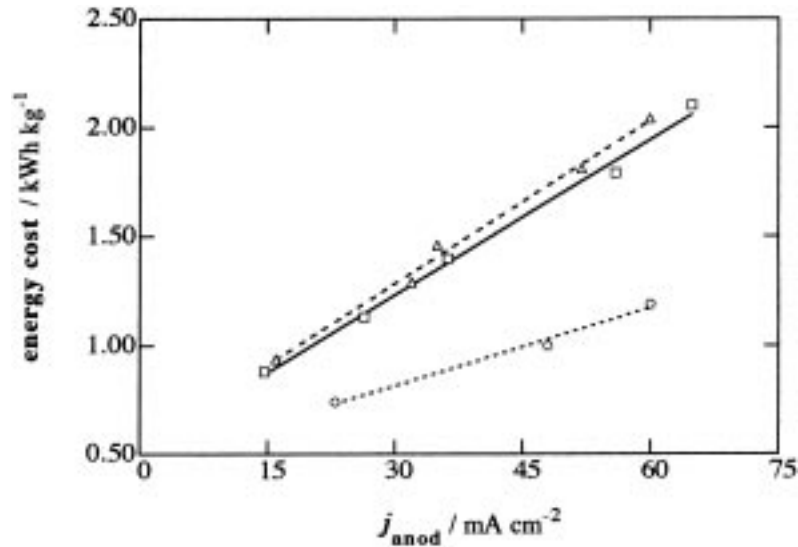
Fig. 6. Change of energy consumption with average anodic current density for the experiments reported in Figure 5.

values of 2.0, 1.7 and 1.4 were always obtained for the sulfate bath at 10, 30 and 50 mA cm^{-2}, respectively. The presence of the magnetic field has little effect on the cell voltage, efficiency and energy cost, although these parameters vary with j. In all media, a decrease in current efficiency with increasing current density is observed. As an example, for the Watts bath, efficiencies of 93%, 83% and 72% were obtained at 10, 30 and 50 mA cm^{-2}, respectively. This progressive loss in efficiency does not occur in the three-electrode system (Figure 5). This behavior can be associated with the lower pH values (< 2) achieved in the two-electrode cell at 30 and 50 mA cm^{-2} due to its lower solution volume. The electrogeneration of a more acidic bath increases the

Table 1. Relative intensities found by XRD for the crystallographic orientations of Ni deposits obtained after 1 h of electrolysis of chloride, Watts and sulfate baths in a two-electrode cell at several current densities in the absence and presence of a magnetic field of 0.9 T oriented either parallel or perpendicular to electrodes

| Bath	j/mA cm^{-2}	Magnetic field	Crystallographic orientation				
			(1 1 1)	(2 0 0)	(2 2 0)	(3 1 1)	(2 2 2)
Chloride	10	–	100	20	14	72	6.3
		parallel	98	13	15	100	6.6
		perpendicular	99	15	22	100	7.5
	30	–	98	16	28	100	9.4
		parallel	66	13	11	100	5.8
		perpendicular	38	5.5	8.0	100	4.5
	50	–	96	18	27	100	7.7
		parallel	43	6.7	28	100	3.8
		perpendicular	48	8.6	7.6	100	3.6
Watts	10	–	100	80	21	28	6.9
		parallel	100	44	17	20	5.4
		perpendicular	100	38	15	16	5.6
	30	–	100	66	41	40	8.4
		parallel	100	60	41	35	6.8
		perpendicular	100	58	40	41	7.8
	50	–	100	61	42	37	6.8
		parallel	100	66	50	40	7.8
		perpendicular	100	67	43	38	7.2
Sulfate	10	–	83	100	75	46	6.6
		parallel	69	77	100	49	7.0
		perpendicular	99	96	100	58	5.2
	30	–	20	29	100	32	1.9
		parallel	7.9	14	100	20	0.0
		perpendicular	7.1	13	100	19	0.0
	50	–	0.3	0.5	100	1.5	0.0
		parallel	0.2	0.3	100	1.0	0.0
		perpendicular	0.3	0.3	100	1.0	0.0
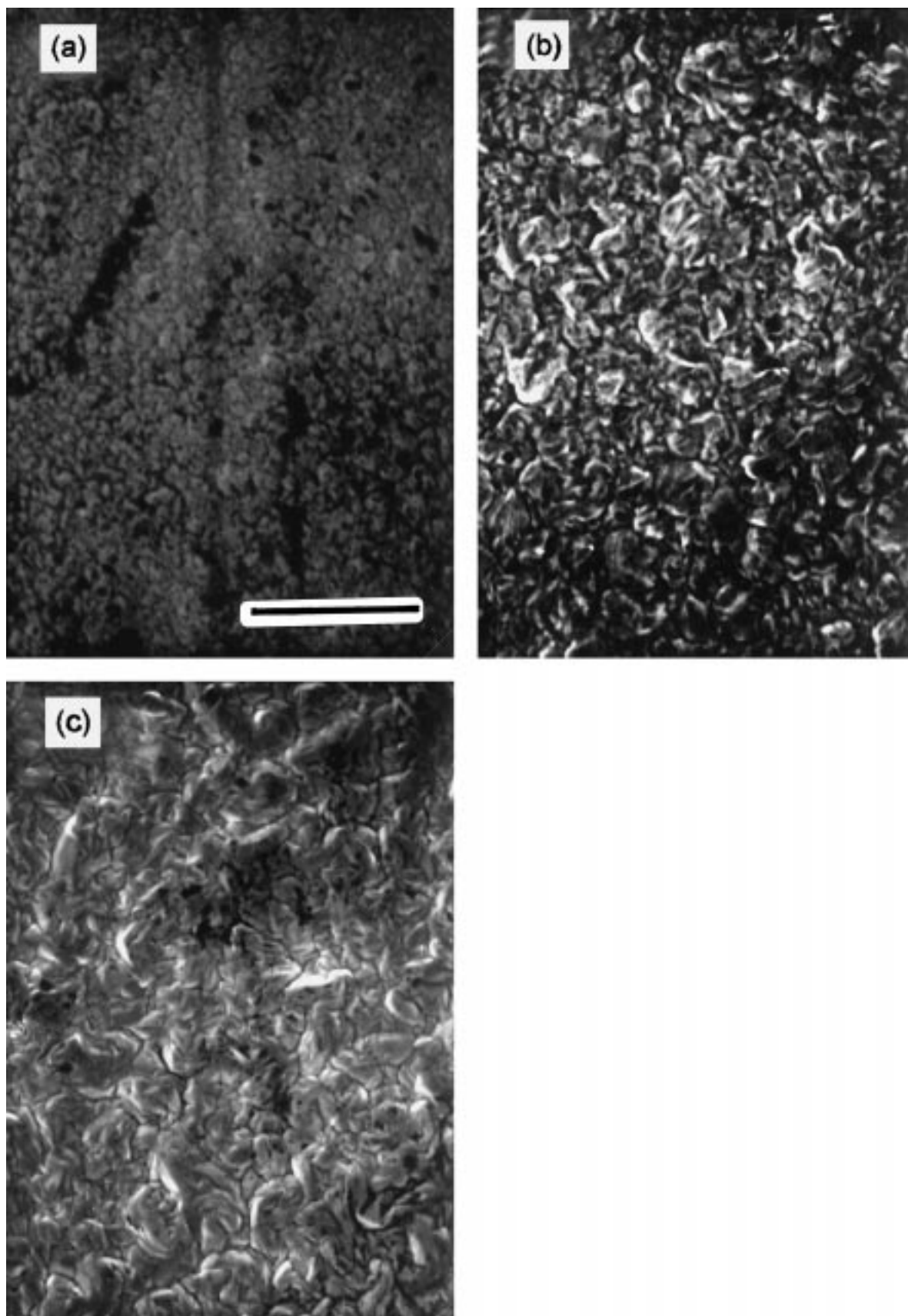
Fig. 7. SEM micrographs of Ni deposits obtained in the two-electrode cell with 50 ml of sulfate bath and without external magnetic field. Current density: (a) 10; (b) 30; (c) 50 mA cm^{-2}. Magnification: (a, c) 730×; (b) 765×. Scale bar 20 μm.
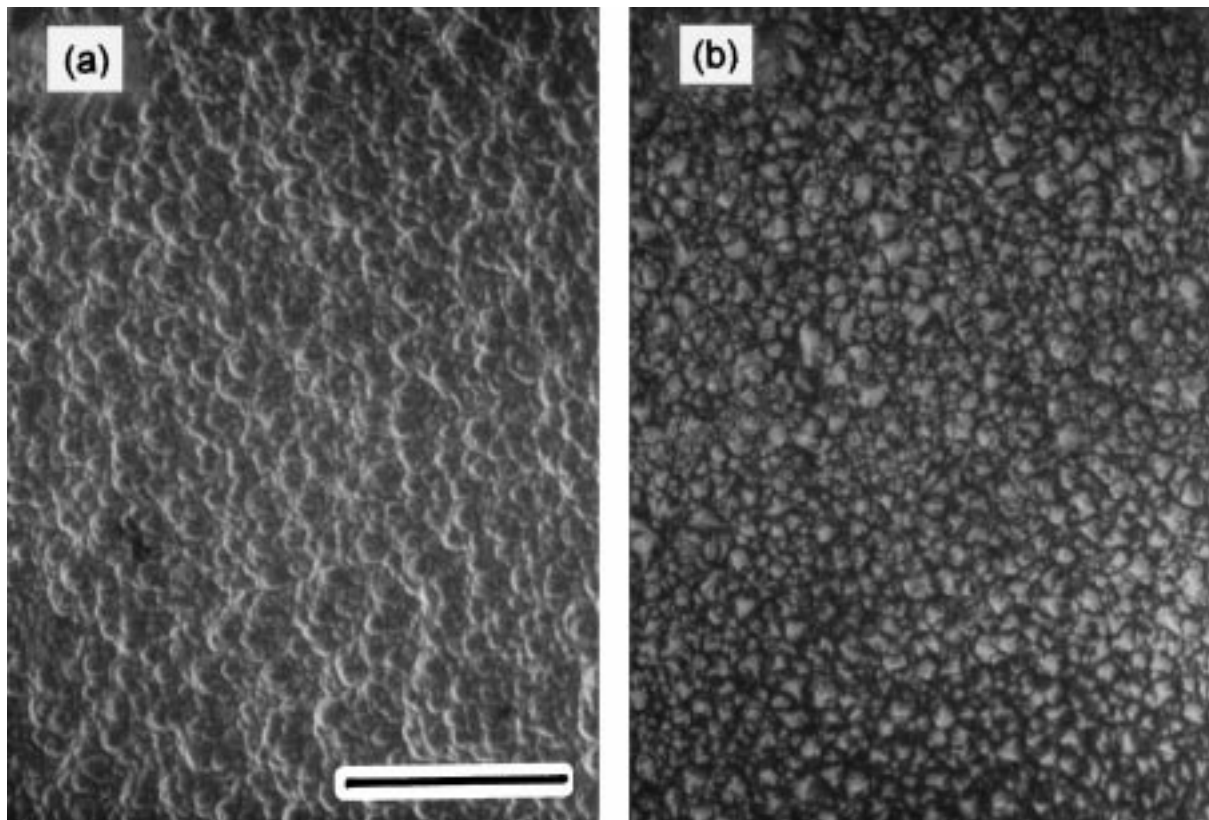
Fig. 8. SEM micrographs of Ni recovered at 50 mA cm^{-2} using the two-electrode cell without external magnetic field. Electrolyte volume 50 ml. (a) Chloride bath; (b) Watts bath. Magnification; (a) 680×; (b) 670×. Scale bar 20 μm.

reduction rate of H$^+$ to H$_2$, then decreasing the efficiency of Ni deposition. The existence of this phenomenon also affects the energy costs. Thus, consumptions of 0.8, 1.4 and 1.7 kWh kg^{-1} for the chloride bath, and of 0.9, 1.5 and 2.2 kWh kg^{-1} for both Watts and sulfate baths, were found at 10, 30 and 50 mA cm^{-2}, respectively. These values are slightly higher than those reported in Figure 6 for the three-electrode cell.

3.3.1. *Purity of deposits*
EDS spectra of all deposits obtained in the two-electrode cell only displayed the bands associated with Ni and centred at 0.85 keV (L band), at 7.47 keV (K_α band) and 8.26 keV (K_β band). This confirms the high purity of recovered Ni, free of heavy metals impurities, such as Pt which may result from anode corrosion, and without contamination of sulfur and/or chlorine from the baths. Chemical analysis of samples by inductively coupled plasm was not carried out because this method has less sensitivity detection of impurities than EDS.

3.3.2. *Crystallographic orientations*
A face-centred cubic structure characterized by the XRD crystallographic planes (1 1 1), (2 0 0), (2 2 0), (3 1 1) and (2 2 2) was determined for all Ni recovered from chloride, Watts and sulfate baths. This crystal structure has also been reported by other authors using similar sulfate [6] and Watts [9] media.

Table 1 summarizes the relative peak intensities of planes found for all baths at different j values in the presence and absence of the magnetic field. The preferred mode of Ni growth mainly depends on the bath and current density. The predominant orientation at 10 mA cm^{-2} without magnetic field is the (1 1 1) plane for both chloride and Watts media, as well as the (2 0 0) plane for the sulfate bath. However, at 30 and 50 mA cm^{-2} with the magnetic field, the preferential orientation is the (3 1 1) plane for the chloride bath and the (2 2 0) plane for the sulfate medium. For the Watts bath, the (1 1 1) orientation predominates in all experimental conditions.

Results of Table 1 for the sulfate bath show that in the absence of magnetic field, the predominance of the (2 2 0) orientation increases with increasing j. When the magnetic field is superimposed, this plane also becomes more predominant, although a higher decay of all peak intensities is always achieved for the perpendicular field. This effect is more noticeable at 10 mA cm^{-2}, where the action of the magnetic field changes the preferential orientation from the (2 0 0) plane to the (2 2 0). At 50 mA cm^{-2}, all minority planes have relative peak intensities lower than 1.6%, indicating that the Ni crystals are formed in the (2 2 0) orientation, in practice.

The effects of current density and magnetic field on crystallographic orientation are not so clear in the other media. For the chloride bath (Table 1), these parameters practically do not affect the (2 2 0) and (2 2 2) planes,
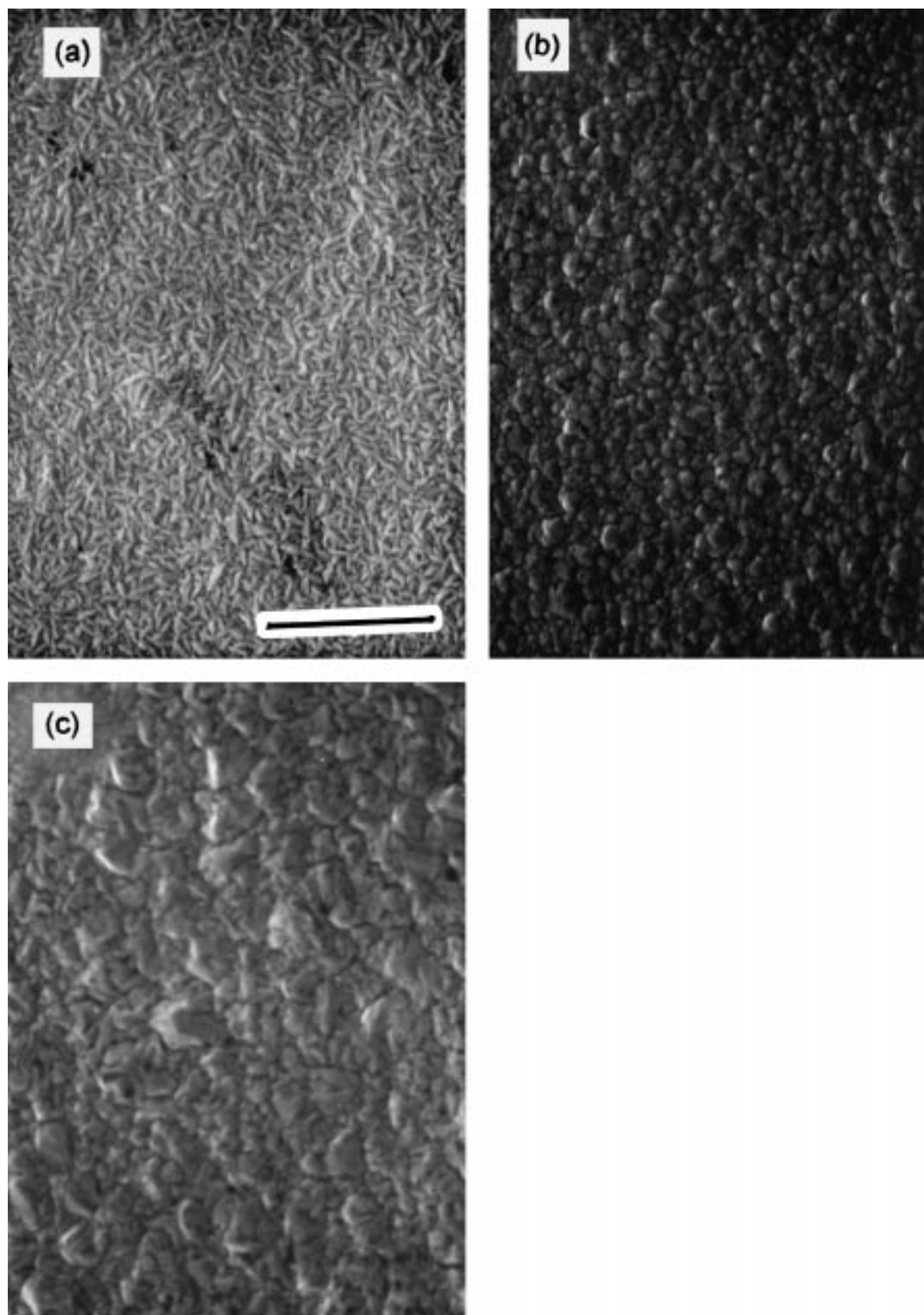
Fig. 9. SEM micrographs recorded after 1 h of Ni electrowinning at 30 mA cm^{-2} when a magnetic field of 0.9 T perpendicular to the electrode surfaces was superimposed to the two-electrode cell. Electrolyte volume 50 ml. (a) Chloride bath; (b) Watts bath; (c) sulfate bath. Magnification: (a) 670×; (b) 660×; (c) 725×. Scale bar 20 μm.

while the (1 1 1) and (2 0 0) orientations diminish in intensity with increasing j, decreasing more quickly when the magnetic field is applied. For the Watts bath, an increase in j gives a slight decay in the (2 0 0) orientation, whereas the other planes are slightly enhanced (Table 1). In this case, a fall in intensity of these planes with the magnetic field is only found at 10 mA cm^{-2}.

3.3.3. Surface morphology
The most notable effect observed by SEM for Ni deposited in the absence of the magnetic field is the increase in grain size with increasing current density, as shown in Figure 7 for the sulfate bath. While small grains are formed at 10 mA cm^{-2} (Figure 7(a)), higher and irregular grains are gradually obtained if j is firstly increased to 30 mA cm^{-2} (Figure 7(b)) and further to 50 mA cm^{-2} (Figure 7(c)). The typical granular morphology at 10 mA cm^{-2} becomes range shaped at 50 mA cm^{-2}. In addition, the Ni deposits from the chloride and Watts baths have lower grain sizes and different morphologies. This can be deduced from comparison of SEM micrographs of Figures 8(a) and (b) obtained at 50 mA cm^{-2} for these baths with that of Figure 7(c) for sulfate. The chloride medium (Figure 8(a)) yields a deposit with a more rounded surface.

The magnetic field enhances the compactness of the Ni grains which grow with more regular sizes and more defined geometrical shapes. Some examples are depicted in Figure 9 for deposits obtained at 30 mA cm^{-2} with the perpendicular field. Well-defined grains of regular size and acicular shape are formed from the chloride bath (Figure 9(a)), a morphology very different from that observed in Figure 8(a) without magnetic field. For the Watts bath, the grains have a more spherical shape in the presence of the field (Figure 9(b)) than in its absence (Figure 8(b)). The sulfate bath also yields more regular grains with better defined geometrical shape with the magnetic field (Figure 9(c)) than without the field (Figure 7(b)).

4. Conclusions

The use of a Pt catalysed H$_2$-diffusion anode for Ni electrowinning has been studied in a three-electrode cell with typical chloride, Watts and sulfate baths at 25 °C. Higher anodic current densities are found when sulfate ions are gradually replaced by chloride ions. The overall process is under ohmic control at high current densities. In the chloride bath, Cl$_2$ is released at the anode and less adherent deposits are formed. Current efficiencies between 94% and 98% for average j_{anod} values ranging from 15 to 65 mA cm^{-2} are always obtained. The energy costs decrease with increasing chloride content, being much lower than those reported for DSA, graphite or lead anodes in chloride and sulfate baths [1–3, 6]. These results suggest that a Pt catalysed H$_2$-diffusion anode is more favourable for Ni electrowinning than the above conventional anodes.

A two-electrode cell placed in a permanent magnet system has been used to study the influence of a magnetic field of 0.9 T on the process. The current efficiency decreases with increasing j from 10 to 50 mA cm^{-2}, because baths become sufficiently acidic to accelerate proton reduction at the cathode. All deposits are composed of high-purity Ni and their crystals have a face-centred cubic structure with a preferential orientation which mainly depends on the electrolyte and current density. The superimposed magnetic field exerts only a small effect on the crystallographic orientation of Ni, although it favours the formation of grains with better defined geometrical shape.

References

1. D.J. Mackinnon, 'The Electrowinning of Metals from Aqueous Chloride' in (ed. by K. Osseo-Asare and J.D. Miller), Conference Proceedings of the Metallurgical Society of AIME, Hydrometallurgy Research, Development and Plant Practice (New York, 1982), p. 659.
2. E. Jackson, 'Hydrometallurgical Extraction and Reclamation' (Horwood, Chichester, 1986), p. 221.
3. Ullmann's, 'Encyclopedia of Industrial Chemistry', 5th edn, Vol. A17 (VCH, Weinheim, 1994), p. 189.
4. J.P. Hoare, J. Electrochem. Soc. 133 (1986) 2491.
5. J. Ji, W.C. Cooper, D.B. Dreisinger and E. Peters, J. Appl. Electrochem. 25 (1995) 642.
6. E. Küzeci, R. Kammel and S.K. Gogia, J. Appl. Electrochem. 24 (1994) 730.
7. V. Nikolova, T. Nikolov, T. Vitanov, A. Möbius, K. Wiesener and D. Schab, J. Appl. Electrochem. 21 (1991) 313.
8. B.C. Banerjee and A. Goswami, J. Electrochem. Soc. 106 (1959) 20 and 590.
9. A. Chiba, K. Kitamura and T. Ogawa, Surf. Coat. Technol. 27 (1986) 83.
10. C. Kollia, N. Spyrellis, J. Amblard, M. Froment and G. Maurin, J. Appl. Electrochem. 20 (1990) 1025.
11. C. Kollia and N. Spyrellis, Surf. Coat. Technol. 57 (1993) 71.
12. A.M. El-Sherik, U. Erb and J. Page, Surf. Coat. Technol. 88 (1996) 70.
13. L. Yang, J. Electrochem. Soc. 101 (1954) 456.
14. A.L. Danilyuk, V.I. Kurmashev and A.L. Matyushkov, Thin Solid Films 189 (1990) 247.
15. R.A. Tacken and L.J.J. Janssen, J. Appl. Electrochem. 25 (1995) 1.
16. O. Devos, A. Olivier, J.P. Chopart, O. Aaboubi and G. Maurin, J. Electrochem. Soc. 145 (1998) 401.
17. A. Hamnett, P.S. Stevens and R.D. Wingate, J. Appl. Electrochem. 21 (1991) 982.
18. E. Brillas, R.M. Bastida, E. Llosa and J. Casado, J. Electrochem. Soc. 142 (1995) 1733.